Design Optimization of Manifold Integrated Skived Cold Plates for Two-Phase Flow-Boiling

Serdar Ozguc, Qingyang Wang, Akshith Narayanan, Jacob Moore, Richard W. Bonner III
Accelsius, Austin, TX, USA
sozguc@accelsius.com

Abstract

Two-phase cooling shows promise for data center applications due to high heat transfer coefficients and heat capacities associated with the boiling phenomena as well as the dielectric nature of the available two-phase coolants. Skived copper cold plates are commonly implemented in data center liquid cooling due to their low cost and ability to achieve fin and channel sizes on the order of 100s of μm. The demand for dissipation of increasing heat fluxes on the next generation of CPU and GPU chips necessitates the need for case-specific design of the cold plate parameters such as channel width, fin thickness, and channel height. To this end, this work performs numerical design optimization of skived cold plates for a set of operating conditions representative of the currently adopted chips in data center applications. Furthermore, a nylon insert to the cold plate package is designed as a manifold to the skived channels to reduce the pressure drop. An empirical convective heat transfer model is developed and calibrated using experimental data collected from two skived cold plates tested under various heat loads and mass flow rates. Developed correlation for the flow-boiling heat transfer coefficient matches with the measured data with less than 20% error. Optimization of the fin thickness and channel width is performed for a range of fin heights and with three different lower bounds on the fin thickness to represent manufacturing constraints. The overall thermal resistance of the optimized cold plates is up to 30% lower than the unoptimized cold plates used during model calibration. Reducing the lower bound on fin thickness enhances the thermal performance, however, reducing the fin thickness limit from 100 to 50 μm provides only a 2% improvement because the overall package resistance is dominated by the thermal interface and base thickness resistances. While thermal performance can be enhanced by incorporating more complex heat transfer features, such as optimized fin and channel shapes and topologies, greater reduction in thermal resistance can be achieved by improving the thermal interface and reducing the copper base thickness.

Nomenclature

D_H	hydraulic diameter, m
f_D	Darcy friction factor, -
G	mass flux, kg/m^2-s
$\bar{h}$	average heat transfer coefficient, W/m^2-K
H_b	base thickness, m
H_f	fin height, m
h_{fg}	latent heat, J/kg
k_s	solid thermal conductivity, W/m-K
L	fin length, m
$\dot{m}$	mass flow rate, kg/s
N	number of fins, -
P_{sat}	saturation pressure, Pa
Q	heat input, W
q''	heat flux, W/m^2
R_{COND}	base conduction resistance, K/W
R_{FB}	flow boiling resistance, K/W
Re	Reynolds number, -
R_{TIM}	TIM resistance, K/W
T_{cp}	cold plate surface temperature, K
t_f	fin thickness, m
T_{sat}	saturation temperature, K
T_w	channel bottom wall temperature, K
W	cold plate width, m
w_c	channel width, m
x_{exit}	exit vapor quality, -
y	position along flow length, m

Greek Symbols

ΔP_{2P}	two-phase pressure drop, Pa
η	fin efficiency, -
μ_f	liquid viscosity, Pa-s
μ_g	vapor viscosity, Pa-s
μ_m	mixture viscosity, Pa-s
ρ_f	liquid density, kg/m^3
ρ_g	vapor density, kg/m^3
ρ_m	mixture density, kg/m^3

Acronyms

CAD	computer aided design
PEEK	polyetheretherketone
TIM	thermal interface material
TTV	thermal test vehicle

Keywords

flow boiling, direct-to-chip cooling, data center cooling, skived cold plates

1. Introduction

The thermal design power of CPU and GPU chips used in data centers are increasing rapidly with the artificial intelligence fueled demand for higher computational power. Currently available Nvidia H100 chips generate up to 700 W of heat [1] in a 814 mm^2 footprint [2]. Densely populated AI rack solutions reach up to 80 kW of power [3]. Two-phase liquid cooling is a potential solution to the thermal management demands of the next generation of data centers due to high heat transfer coefficients and heat capacities associated with boiling as well as the dielectric nature of the available two-phase coolants. Thermal resistance of the cold plates in a two-phase cooling system impacts the available heat dissipation at the maximum operating temperature, making it crucial to design efficient cold plates that enhance heat removal.

Numerical optimization of heat sinks and cold plates have been shown to provide significant performance improvements relative to intuition-based designs [4, 5, 6]. However, commonly adopted gradient-based algorithms rely on numerical models of the governing physics to calculate the gradients of the cost function with respect to the design variables. This poses a challenge for optimization of

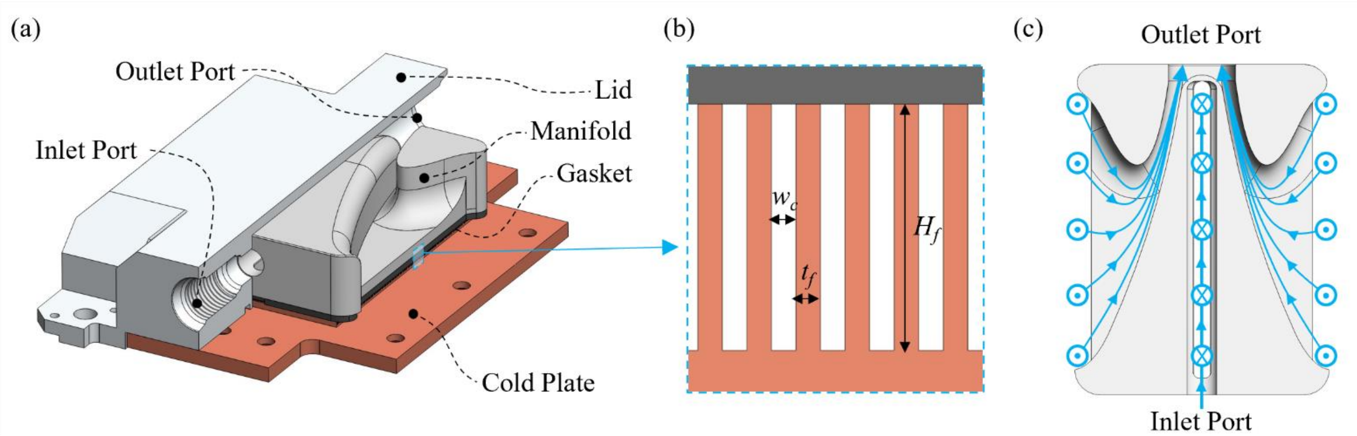

Figure 1. (a) Drawing of the TTV assembly with the aluminum lid cut-sectioned in half. (b) Side-view drawing of the skived fins with geometric parameters labeled. (c) Top-down cut-section view of the manifold with flow paths drawn (x symbols representing into the page, • out of the page).

components under flow-boiling because the available modeling approaches are highly specific to geometry and operating conditions. Flow-boiling models can be calibrated using experimental data prior to optimization to generate meaningful results [7].

Manufacturing capabilities need to be captured in the formulation of the design variables and the constraints. Skived copper cold plates are commonly implemented in data center liquid cooling due to their low cost and ability to achieve fin and channel sizes on the order of 100s of microns, which is critical to the cooling performance. However, design optimization of skived fin cold plates for two-phase cooling in data center applications is limited in literature. To this end, this study aims to generate optimized skived cold plates under flow-boiling with minimized thermal resistance. An insert to the lid is designed as a manifold to the skived channels to reduce the pressure drop across the cold plate, resembling a two-layer manifold heat sink commonly adopted in literature [8, 9, 10]. A numerical flow-boiling model is used for size optimization of the skived fins. To produce a reference dataset to calibrate the numerical model, the thermal resistances of different skived cold plates with various fin and channel sizes are experimentally measured under flow-boiling. The performances of the optimized cold plates are then investigated.

2. Methodology

Optimization results are dependent on the operating conditions and geometric constraints, which are summarized as follows. A cold plate with a finned footprint area of 60.2 mm × 41 mm is investigated. Uniform heating of 1 kW is applied along the bottom surface. The chosen working fluid is refrigerant R515B **[**11**]**, which enters the cold plate, flows through the channels between the skived fins, and boils at 30°C while absorbing the heat as it changes phase. The target exit vapor quality is $x_{exit} = 0.7$, which corresponds to a mass flow rate of $\dot{\boldsymbol{m}} = 9.02$ g/s.

2.1. Experimental Methods

Experimental data are needed to calibrate the numerical models used during optimization. To this end, a thermal test vehicle (TTV) is designed to emulate the boundary conditions of the investigated cold plate. Figure 1a shows a drawing of the TTV assembly with the aluminum lid cut-sectioned in half to show the internal components. The skived copper cold plate is bolted to the lid. Ports placed on the opposite sides of the lid act as the inlet and outlet respectively for refrigerant to flow through the cold plate. A copper block, not shown in the drawing, is compressed against the bottom surface of the cold plate with a thermal interface material (TIM) in between. Four cylindrical cartridge heaters inserted into the copper block generate heat, which transfers from the heater block to the cold plate through the TIM. The copper block is seated inside an insulating PEEK block to reduce heat losses to ambient. Thermocouples are inserted into the copper block and at the bottom surface of the cold plate, each centered within the heated area. Figure 1b shows a side-view drawing of the skived fins with the geometric parameters labeled where w_c is the channel width, t_f is the fin thickness, and H_f is the fin height.

A nylon manifold is placed inside the lid. Figure 1c illustrates a top-down cut-section of the manifold, with arrows depicting the flow path and symbols representing flow into and out of the page. Refrigerant enters through the inlet port and flows toward the outlet port, where a thin wall obstructs the direct path. This forces the refrigerant downward to the cold plate, where it splits into two outward directions within the channels. The channels augment the area over which heat transfer occurs and create a forced flow condition for the now-boiling refrigerant. The resulting liquid-vapor mixture exits the channels and flows back inward to the outlet port via the manifold. The manifold's geometry effectively divides the flow, reducing pressure drop by shortening the flow path. A gasket cut to match same profile of the bottom surface of the manifold is placed between the manifold and the fins to ensure the flow is directed through the channels rather than over them.

A two-phase flow loop is built to produce and control the operating conditions inside the TTV. Figure 2 shows a schematic diagram of the flow loop. Liquid refrigerant inside a reservoir is pumped through the loop with a gear pump (Micropump L28640). Refrigerant is pushed through an orifice before entering the TTV to suppress flow-boiling instabilities by inducing a large pressure drop upstream. Then, refrigerant flows through the TTV where it boils, and the resulting liquid-

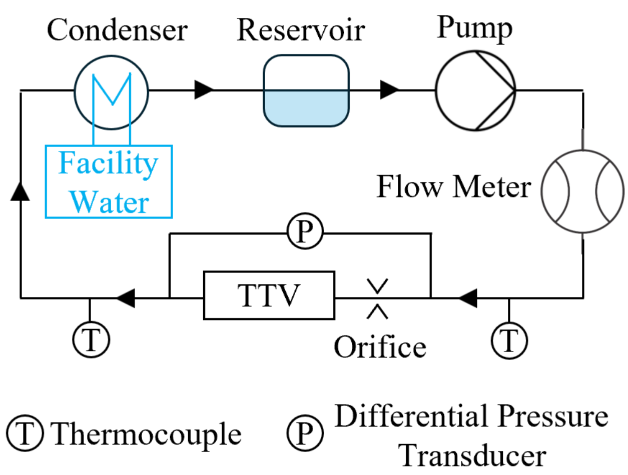

Figure 2. Schematic diagram of the flow loop.

vapor mixture condenses inside a brazed plate heat exchanger condenser. The heat is removed from the system by the facility water in a secondary loop. The condensed refrigerant flows back into the reservoir. The reservoir acts as a buffer for the changes in vapor volume in the system. Temperatures are measured before and after the TTV using thermocouple probes inserted into the flow. The pressure drop across the TTV is measured using a differential pressure transducer (Omega PX409-015DWU10V). An ultrasonic flow meter (Keyence FD-XS8) placed between the pump and the TTV measures the volumetric flow rate of the liquid refrigerant.

The flow loop and TTV enable the control of flow rate with the gear pump, heat input with a thyristor-based power controller (Gefran GFX4-IR) connected to the cartridge heaters, and boiling temperature by adjusting the facility water flow rate. Subcooling at the inlet of the TTV is not controlled but rather is an artifact of the vapor-line pressure drop in the loop. Subcooling was ensured to be below 5°C throughout all testing. Thermocouples and pressure transducer signals are measured and recorded using a data acquisition system (Keysight DAQ970A with DAQM901A). All data collection is performed at 1 Hz and averaged over a one-minute period to smooth out short-term fluctuations.

Two skived cold plates with different fin sizes are experimentally tested to collect model calibration data. Figure 3 shows side-view microscope images of the skived fins of (a) cold plate #1 and (b) cold plate #2. As a result of the skiving process, the fins are not purely rectangular as depicted in the CAD image in Figure 1a; instead, they are thicker near the base and thinner near the top. Cold plate #1 has fins with pointy tips, and cold plate #2 has curved fins. To reduce complexity of the model, numerical modeling is conducted based on the assumption of rectangular fins and channels, where the fin thickness and channel width are measured from the center along the height and averaged across all the fins shown in Figures 3a and 3b. Table 1 summarizes the geometric dimensions where H_b is the solid base thickness between the fins and the heated surface.

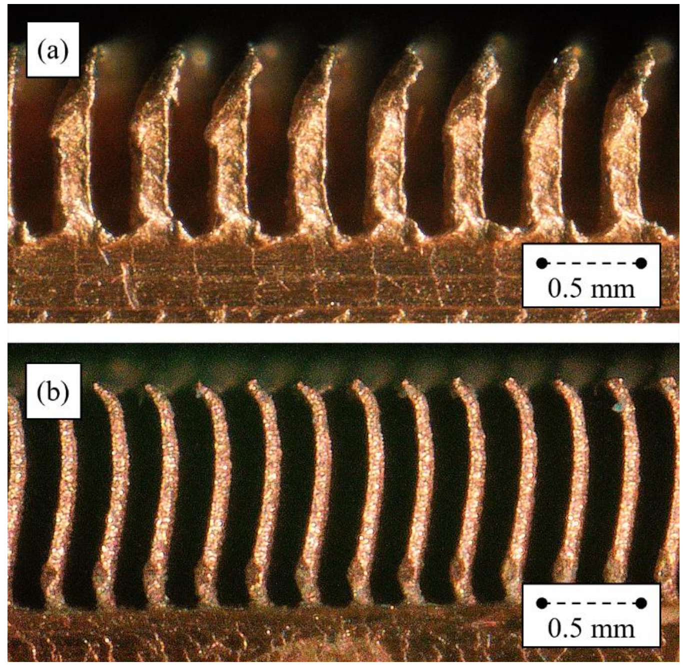

Figure 3. Side-view optical images of the skived fins of (a) cold plate #1 and (b) cold plate #2.

Table 1. Dimensions of the two cold plates tested.

#	t_f [mm]	w_c [mm]	H_f [mm]	H_b [mm]
1	0.20	0.20	0.94	4.54
2	0.10	0.15	0.13	4.08

Calibration data are collected over a range of operating conditions. The cold plates are tested at various heat inputs (Q) between 0-1 kW. Exit vapor qualities (x_{exit}) between 0-1 are achieved by varying refrigerant flow rate for a given heat input. Boiling temperature is kept between 25-30°C, and subcooling is kept below 5°C for all tests. A total of 37 tests are conducted where heater temperature (T_h), cold plate bottom surface temperature (T_{cp}), inlet refrigerant temperature (T_{in}), outlet refrigerant temperature (T_{out}), and pressure drop across the cold plate (ΔP) are measured.

2.2. Numerical Methods

The overarching objective of the optimization is to lower the junction temperature of high heat flux chips in data centers. To this end, the overall thermal resistance of the cold plate package (R) is minimized. Thermal resistance is divided into three subcomponents: thermal resistance across the TIM (R_{TIM}), conduction resistance across the copper base thickness between the TIM and the fins (R_{COND}), and the thermal resistance through the fins and between the fins and the boiling refrigerant (R_{FB}). R_{TIM} is constant for a given heated surface area and therefore is not included in the optimization objective. Similarly, R_{COND} is assumed constant because heat input is uniform and convective resistance across the finned surface is expected to be uniform under boiling (i.e., heat spreading is negligible). Therefore, the objective is formulated as follows.

$$\min_{w_c, t_f} R_{FB}(w_c, t_f) \quad [1]$$

$$R_{FB} = \frac{T_w - T_{sat}}{Q} \quad [2]$$

where T_w is the bottom wall temperature of the channels, and T_{sat} is the saturation temperature of the refrigerant at the outlet of the cold plate. The design variables w_c and t_f are to be optimized to minimize the flow-boiling thermal resistance R_{FB}.

Flow-boiling thermal resistance is estimated using an average heat transfer coefficient for flow boiling ($\bar{h}$) and the extended surface analysis from Incropera et al. [12] wherein the effective surface area provided by the fins is a fraction of the total surface are defined by the fin efficiency (η).

$$R_{FB} = \frac{1}{\bar{h}NL(w_c + 2H_f\eta)} + \frac{dT_{sat}}{dP_{sat}}\frac{\Delta P_{2P}}{Q} \quad [3]$$

$$\eta = \frac{\tanh\left(H_f\sqrt{2\bar{h}/k_s t_f}\right)}{H_f\sqrt{2\bar{h}/k_s t_f}} \quad [4]$$

where N is the number of fins across the width (W = 60.2 mm), L is the length of the fins along the cold plate (L = 41 mm), and k_s is the thermal conductivity of the copper (388 W/m-K). The last term in Equation 3 represents the resistance arising from the increase in saturation temperature caused by the frictional pressure drop resulting from the two-phase flow within the channels (ΔP_{2P}). Pressure drop due to acceleration is calculated to be negligible for the investigated cold plate geometries, heat inputs, and mass flow rates. The term dT_{sat}/dP_{sat} is the gradient of saturation temperature with respect to saturation pressure and is equal to 0.41 K/psi at the saturation temperature of 30°C used throughout this study.

The pressure drop inside the channels is estimated by using the following assumptions. The flow is laminar and fully developed. Two-phase mixture is homogeneous, i.e., liquid and vapor phases are at equal speed. A mixture modeling approach [12] is used with the Darcy-Weisbach equation as follows.

$$\frac{dP_{2P}}{dy} = \frac{(f_D Re)\mu_m \dot{m}}{2\rho_m N w_c H_f D_H^2} \quad [5]$$

where y is the position along the flow length inside a channel, f_D is the Darcy friction factor, Re is the Reynolds number, μ_m is the mixture viscosity, $\dot{m}$ is the mass flow rate across the cold plate, ρ_m is the mixture density, and D_h is the hydraulic diameter. The optimized channels are expected to have high aspect ratio; therefore, value of 96 is used for $f_D Re$ [13] and $D_h = 2w_c$, which corresponds to flow between parallel plates. The mixture viscosity is estimated using the correlation by McAdams et al. [14] and the mixture density is calculated as follows.

$$\frac{1}{\rho_m} = \frac{1-x}{\rho_f} + \frac{x}{\rho_g} \quad [6]$$

$$\frac{1}{\mu_m} = \frac{1-x}{\mu_f} + \frac{x}{\mu_g} \quad [7]$$

where x is the local vapor quality, and subscripts f and g represent liquid and vapor phases respectively. Heat dissipation by the refrigerant is assumed to be uniform along the flow length. Therefore, the vapor quality increases linearly along the flow position and Equation 5 is integrated across the channel as follows.

$$\Delta P_{2P} = \frac{L(f_D Re)\dot{m}}{4Nw_c H_f D_H^2 x_{exit}}\int_0^{x_{exit}} \frac{\mu_m}{\rho_m}dx \quad [8]$$

where x_{exit} is the vapor quality at the outlet of the cold plate.

The heat transfer coefficient in Equation 3 is to be calibrated using the experimental measurements taken from the two skived cold plates tested. Therefore, a general formulation is used for the average heat transfer coefficient as follows.

$$\bar{h} = C_1 q"^{C_2} G^{C_3} w_c^{C_4} x_{exit}^{C_5}(1 - x_{exit})^{C_6} \quad [9]$$

$$q" = \frac{Q}{NL(w_c + 2H_f\eta)} \quad [10]$$

where q" is the heat flux at the fin walls, G is the mass flux in the channels, and C_1-C_6 are the model coefficients which are determined by curve fitting Equation 9 to the heat transfer coefficients calculated from the experimental measurements. The definition of heat flux provided in Equation 10 contains the term η (Equation 4) which is a function of $\bar{h}$. Therefore, when the thermal resistance is calculated during curve fitting and design optimization, Equation 9 is solved iteratively with an initial guess of $\eta = 1$ until convergence.

Calibration of the model coefficients requires calculation of the heat transfer coefficient from the experimental measurements which can be achieved using Equations 2-4, 9, and 10. However, T_w in Equation 2 (the bottom wall temperature of the channels) is not directly measured during testing. Instead, T_{cp}, cold plate bottom surface temperature, is measured and T_w is estimated assuming 1D conduction across the solid cold plate base as follows.

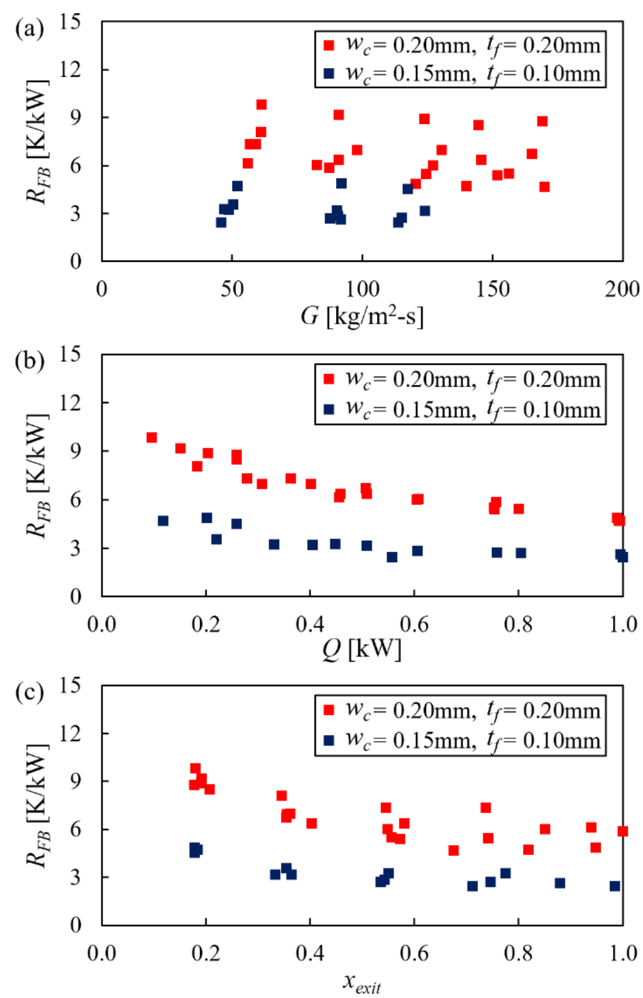

Figure 4. Thermal resistance with respect to mass flux, heat input, and exit quality for the two cold plates tested.

$$T_w = T_{cp} - \frac{QH_b}{k_s LW} \quad [11]$$

The optimization problem formulated in Equation 1 is solved using the interior-point algorithm. Constant-value properties of R515B evaluated at 30°C are used throughout the calibration and optimization, which are shown in Table 2.

Table 2. Properties of R515B at 30°C [15].

ρ_f [kg/m^3]	ρ_g [kg/m^3]	μ_f [μPa-s]	μ_g [μPa-s]	h_{fg} [kJ/kg]
1163.9	31.3	181.3	12.5	158.2

3. Results

Two skived cold plates were tested under various flow rates and heat inputs for a total of 37 experiments. Figure 4 shows the flow boiling thermal resistance plots with respect to mass flux, heat input, and exit vapor quality. Thermal resistance decreases with higher heat input and exit vapor quality. However, the three variables are not independent; exit vapor quality is calculated from the mass flux and heat input. Therefore, the reduction in thermal resistance at higher exit vapor qualities may be attributed to the increased heat loads required to achieve those higher qualities or vice versa. Thermal resistance shows a significant dependence on the cold plate dimensions, as seen by the noticeable offset in resistances between the two cold plates.

Heat transfer coefficient correlation shown in Equation 9 is fit to the experimental data by optimizing the six coefficients to minimize the mean-square-error between measurements and predictions. Coefficients C_3 and C_6 resulted in small values and therefore are dropped to further simply the equation without significant loss in prediction accuracy. The equation below shows the resulting heat transfer coefficient correlation after calibration.

$$\bar{h} = 90.46 q''^{0.27} w_c^{-1.32} x_{exit}^{0.11} \quad [12]$$

where all variables are defined in SI units except w_c which is in millimeters. Figure 5 compares the measured heat transfer coefficient with the predictions from Equation [12]. The predictions closely match the measurements, within 20% error bounds. However, it is important to note that this correlation is specific to the boundary and operating conditions investigated in this study.

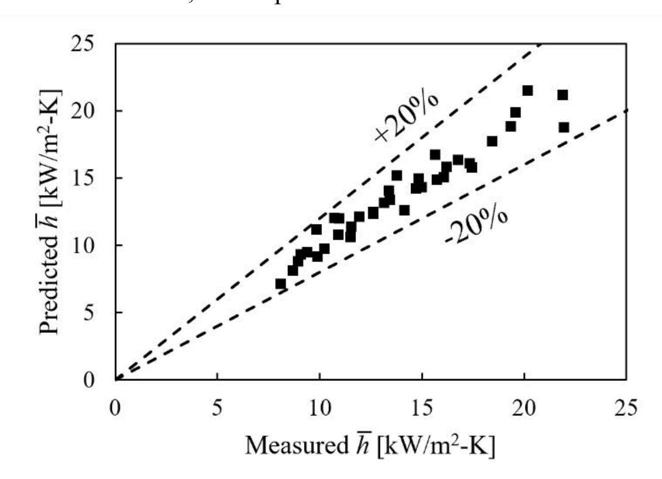

Figure 5. Measured average heat transfer coefficient vs prediction by the calibrated model.

The minimum fin thickness achievable by the skiving process is limited. Therefore, optimization defined in Equation 1 is performed with a lower bound on the fin thickness. Three different lower bounds of 0.2, 0.1, and 0.05 mm are used to capture the effect of the lower bound on the optimal performance. The commercially advertised limit is represented by 0.2 mm, minimum fin thickness achieved by fine-tuning the skiving process by the authors is 0.1 mm, and 0.05 mm is investigated to understand the performance implications of producing thinner fins. Figure 6a shows the flow boiling thermal resistance of the cold plates optimized at varying fin heights (H_f = 0.2-2.5 mm) and for three different lower bounds on fin thickness. Thermal resistance is decreasing with increasing fin height as more surface area becomes available and pressure drop is reduced by the larger available flow area. The fin efficiency defined in Equation 4 decreases with fin height. Therefore, thermal resistance asymptotes at higher fin heights, providing diminishing returns. The optimized fin thickness is calculated to always match the lower bound, indicating that a fin thickness smaller than the imposed lower bound is preferred for optimal thermal performance. The difference in thermal resistance between the three lower bounds is small at higher fin heights, reaching R_{FB} = 1.13, 0.89, and 0.74 K/kW for $t_f \geq$ 0.2, 0.1, and 0.5 mm, respectively, at a fin

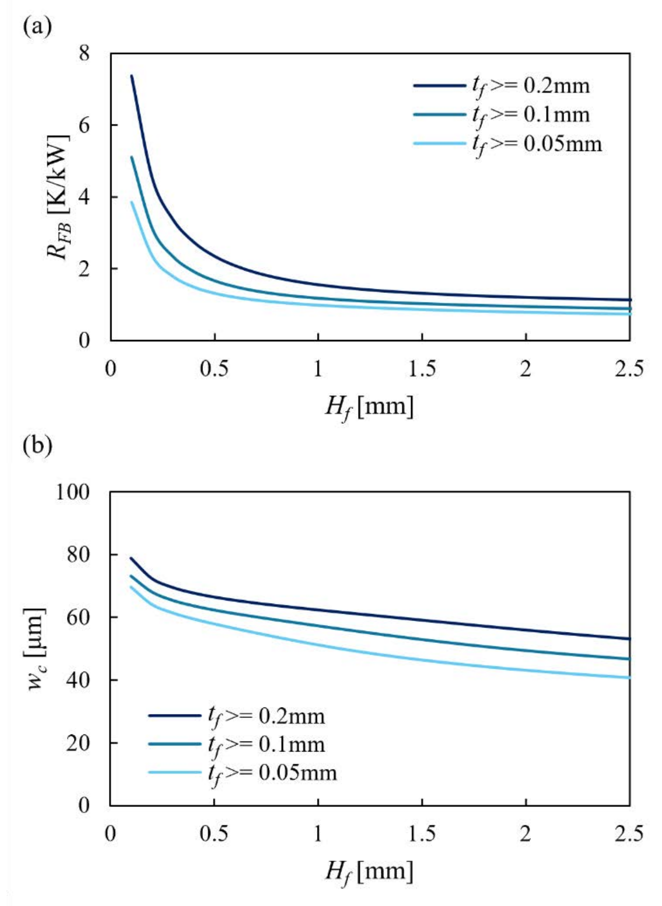

Figure 6. (a) Thermal resistance and (b) channel width of the cold plates optimized at various fin heights and fin thickness bounds.

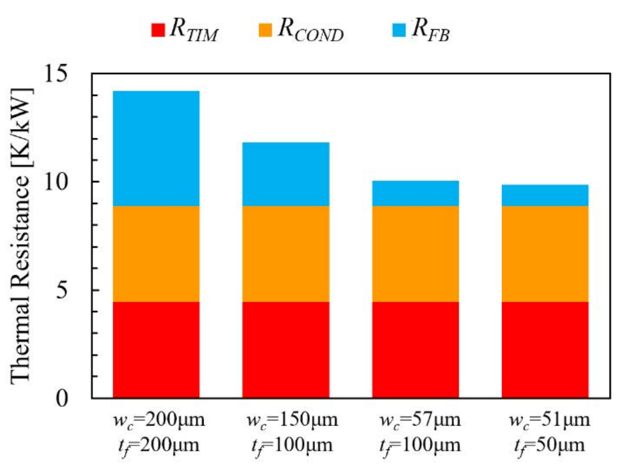

Figure 7. Overall thermal resistance stack-up for four cold plates with different channel widths and fin thicknesses.

height of 2.5 mm. Therefore, the benefit of using thinner fins diminishes with increasing fin height. Figure 6b shows the channel widths for the optimized thermal resistances shown in Figure 6a. Optimized channel width is less than 0.1 mm throughout and decreases with increasing fin height. Also, the channel width is smaller when a lower bound on fin thickness is used indicating that a smaller channel is preferred for thinner fins.

Thermal resistance of the overall packaging is investigated to evaluate the performance enhancement provided by the optimization. Figure 7 shows thermal resistance stack-up for four different cold plates, each with a fin height of 1 mm. Cold plates with 200 µm and 150 µm channel width represent the two cold plates fabricated and tested. The other two bars belong to the cold plates optimized using a fin height of 1 mm with the two of the lower bounds on fin thickness (0.1 and 0.05 mm). Flow boiling thermal resistance, R_{FB}, is calculated using the calibrated model. Base conduction resistance, R_{COND}, is estimated to be 4.43 K/kW assuming 1D conduction across a 4 mm copper thickness. Thermal resistance across the TIM, R_{TIM}, is measured to be 4.44 K/kW during experimentation of the two cold plates. R_{COND} and R_{TIM} are estimated to be equal between all cold plates because the same TIM and base thickness are used, and heat spreading is assumed negligible. Predictions of the flow boiling thermal resistances of the optimized cold plates are significantly lower than those of the two cold plates tested (60-80% reduction). Likewise, the overall thermal resistances of the optimized cold plates are significantly lower than those of the two cold plates tested, with a 30% reduction between the worst and best performers. The flow-boiling-related component of the thermal resistance reduces by 15% between the two optimized cold plates due to the difference in fin thickness. However, this difference shrinks to only 2% when the overall resistance of the package is considered.

4. Conclusions

Optimization of skived cold plates is investigated for direct-to-chip two-phase cooling for data centers using refrigerant R515B. A numerical model of flow-boiling in skived cold plates is developed and calibrated using experimental measurements. Optimization of the channel width and fin thickness is performed. The predicted thermal resistances of the optimized cold plates are then compared to the experimentally measured resistances of the unoptimized cold plates. Conclusions are summarized as follows.

- Average heat transfer coefficient for flow-boiling in skived cold plates is strongly dependent on the heat flux, exit vapor quality, and channel width. Mass flux of refrigerant does not have a significant impact on the heat transfer coefficient for the operating conditions and the cold plate dimensions investigated.
- Optimized fin thicknesses are always equal to the enforced lower bounds, imposed by manufacturability rules of thumb. Thermal resistance is lower when the lower bound is reduced, however, the performance enhancement for using a smaller fin thickness limit diminishes at higher fin heights.
- Smaller channels provide higher heat transfer coefficients, however, the increase in pressure drop increases the boiling temperature and thermal resistance. Therefore, optimized channel width is smaller when the fin thickness is reduced or fin height is increased, both of which provide more flow area and enable the smaller channels without causing a detrimental increase in pressure drop.
- Optimization of the channel width and fin thickness offers significant reduction to R_{FB}, the flow-boiling resistance. The optimized cold plate with 50 µm fin thickness and 51 µm channel width has 80% lower flow boiling resistance compared to the fabricated 200 µm fin thickness and 200 µm channel width. However, the improvement reduces to 30% when the overall thermal resistance consisting of the TIM and the copper base is considered.
- Reducing the fin thickness of optimized cold plates from 100 to 50 µm provides a 15% reduction in flow boiling thermal resistance. The improvement reduces to 2% when overall package resistance is considered because the resistance of the TIM and the cold plate base thickness dominate. For the optimized cold plates, flow boiling thermal resistance accounts for as small as 10% of the cold plate assembly resistance. Therefore, further improvements to the cold plate performance for two-phase direct-to-chip cooling in data centers will come from reducing the TIM and base conduction resistances.

References

[1] "NVIDIA H100 Tensor Core GPU," Nvidia. Accessed: Sep. 26, 2024. [Online]. Available: https://resources.nvidia.com/en-us-tensor-core/nvidia-tensor-core-gpu-datasheet

[2] "NVIDIA H100 PCIe 80 GB." TechPowerUp. Accessed: Sep. 26, 2024. [Online]. Available: https://www.techpowerup.com/gpu-specs/h100-pcie-80-gb.c3899#:~:text=Since%20H100%20PCIe%2080%20GB,mm%C2%B2%20and%2080%2C000%20million%20transistors

[3] "Large Language Models (LLM) to the AI Edge," Super Micro. Accessed: Sep. 26, 2024. [Online]. Available: https://www.supermicro.com/manuals/brochure/Brochure_AI_GPU_Workloads.pdf

[4] K. L. Kirsch and K. A. Thole, "Numerical Optimization, Characterization, and Experimental Investigation of Additively Manufactured Communicating

Microchannels," *J. Turbomach.*, vol. 140, no. 11, p. 111003, Nov. 2018, doi: 10.1115/1.4041494.

[5] J. H. Ryu, D. H. Choi, and S. J. Kim, "Three-dimensional numerical optimization of a manifold microchannel heat sink," *Int. J. Heat Mass Transf.*, vol. 46, no. 9, pp. 1553–1562, Apr. 2003, doi: 10.1016/S0017-9310(02)00443-X.

[6] S. Ozguc, L. Pan, and J. A. Weibel, "Optimization of permeable membrane microchannel heat sinks for additive manufacturing," *Appl. Therm. Eng.*, vol. 198, p. 117490, Nov. 2021, doi: 10.1016/j.applthermaleng.2021.117490.

[7] S. Ozguc, L. Pan, and J. A. Weibel, "An approach for topology optimization of heat sinks for two-phase flow boiling: Part 1 – Model formulation and numerical implementation," *Appl. Therm. Eng.*, vol. 249, p. 123337, Jul. 2024, doi: 10.1016/j.applthermaleng.2024.123337.

[8] D. Copeland, H. Takahira, W. Nakayama, and B.-C. Pak, "Manifold microchannel heat sinks: theory and experiments," *Adv. Electron. Packag.*, vol. 10, no. 2, pp. 829–834, 1995.

[9] M. A. Arie, A. H. Shooshtari, S. V. Dessiatoun, E. Al-Hajri, and M. M. Ohadi, "Numerical modeling and thermal optimization of a single-phase flow manifold-microchannel plate heat exchanger," *Int. J. Heat Mass Transf.*, vol. 81, pp. 478–489, Feb. 2015, doi: 10.1016/j.ijheatmasstransfer.2014.10.022.

[10] I. L. Collins, J. A. Weibel, L. Pan, and S. V. Garimella, "A permeable-membrane microchannel heat sink made by additive manufacturing," *Int. J. Heat Mass Transf.*, vol. 131, pp. 1174–1183, Mar. 2019, doi: 10.1016/j.ijheatmasstransfer.2018.11.126.

[11] "Solstice N15 (R-515B) Technical Data Sheet," Honeywell. Accessed: Jan. 01, 2025. [Online]. Available: https://www.honeywell-refrigerants.com/europe/wp-content/uploads/2022/01/Solstice-N15-TDS_EN.pdf

[12] W. Chao-Yang and C. Beckermann, "A two-phase mixture model of liquid-gas flow and heat transfer in capillary porous media—I. Formulation," *Int. J. Heat Mass Transf.*, vol. 36, no. 11, pp. 2747–2758, Jul. 1993, doi: 10.1016/0017-9310(93)90094-M.

[13] *F. P. Incropera, D. P. DeWitt, T. L. Bergman, A. S. Lavine, "Fundamentals of Heat and Mass Transfer," Wiley, 2011*.

[14] W. H. McAdams, W. K. Woods, and L. C. Heroman, "Vaporization Inside Horizontal Tubes—II Benzene-Oil Mixtures," *J. Fluids Eng.*, vol. 64, no. 3, pp. 193–199, Apr. 1942, doi: 10.1115/1.4019013.

[15] M. Huber, A. Harvey, E. Lemmon, G. Hardin, I. Bell, and M. McLinden, "NIST Reference Fluid Thermodynamic and Transport Properties Database (REFPROP) Version 10 - SRD 23." National Institute of Standards and Technology, 2018. doi: 10.18434/T4/1502528.